NASA TECHNICAL NOTE

NASA TN D-3104

NASA TN D-3104

INFLUENCE OF THE BUMPER AND MAIN WALL MATERIAL ON THE EFFECTIVENESS OF SINGLE METEOROID BUMPERS

by Donald H. Humes

Langley Research Center
Langley Station, Hampton, Va.

NATIONAL AERONAUTICS AND SPACE ADMINISTRATION - WASHINGTON, D. C. - NOVEMBER 1965

NASA TN D-3104

INFLUENCE OF THE BUMPER AND MAIN WALL MATERIAL ON THE EFFECTIVENESS OF SINGLE METEOROID BUMPERS

By Donald H. Humes

Langley Research Center
Langley Station, Hampton, Va.

NATIONAL AERONAUTICS AND SPACE ADMINISTRATION

For sale by the Clearinghouse for Federal Scientific and Technical Information
Springfield, Virginia 22151 -- Price $2.00

INFLUENCE OF THE BUMPER AND MAIN WALL MATERIAL ON THE EFFECTIVENESS OF SINGLE METEOROID BUMPERS

By Donald H. Humes
Langley Research Center

SUMMARY

An experimental investigation was conducted to determine the relative effectiveness of single aluminum, beryllium, lead, magnesium, Mylar, neoprene, and stainless-steel meteoroid bumpers and the relative effectiveness of aluminum, beryllium, lead, magnesium, and stainless-steel main walls in reducing the total penetration damage produced by 1.59-mm-diameter aluminum projectiles at velocities up to 5.88 km/s.

The maximum total penetration damage was found to be a function of the mass per unit area of the bumper and to be independent of the bumper material. The maximum total penetration damage and the optimum bumper mass were functions of the main wall material, the less dense main wall materials being generally more effective. The optimum bumper mass against the 1.59-mm-diameter aluminum projectiles was independent of the bumper material and was approximately 1 kg/m^2 when a finite-thickness aluminum main wall was used and 3 kg/m^2 when a finite-thickness lead main wall was used.

INTRODUCTION

It was first proposed by Whipple (see ref. 1) that the penetration damage inflicted on a spacecraft by meteoroids could be greatly reduced by placing a thin shield a short distance from the main structure of the spacecraft. Whipple suggested that meteoroids would be extensively fragmented or even vaporized during penetration of the thin shield, most often referred to as a meteoroid bumper, and that the resulting debris would impact over a large area of the main structure and inflict only slight damage. Reference 2 shows that aluminum and copper projectiles could be fragmented during penetration of an aluminum meteoroid bumper, if the bumper thickness were properly chosen and the impact velocity were sufficiently high.

This investigation was conducted to determine the relative effectiveness of several bumper and main wall materials in reducing the impact damage of spherical aluminum projectiles at velocities up to 5.88 km/s and by this means to discover the desired material properties of a bumper and main wall. Aluminum spheres 1.59 mm in diameter were used as projectiles. In order to determine the important bumper properties, impact data were obtained for aluminum,

beryllium, lead, magnesium, Mylar, neoprene, and stainless-steel bumpers. Bumper thicknesses ranged from 0.025 mm to 6.35 mm. A large standoff distance of 51mm (32 projectile diameters) was used to separate the bumper from the quasi-infinite aluminum main wall. In order to determine the important main wall properties, impact data were obtained for unprotected quasi-infinite aluminum, beryllium, lead, magnesium, and stainless-steel main walls.

SYMBOLS

d	projectile diameter
F	ratio of maximum single plate thickness which can be completely penetrated to penetration depth in single quasi-infinite plate under the same impact condition
h	standoff distance
m	mass per unit area
P	penetration depth
R_x	ratio of the penetration damage to an unprotected quasi-infinite main wall $(P_{mw}\rho_{mw})$ when a general main wall material is used, to the damage occurring when an unprotected quasi-infinite aluminum main wall is used under the same impact conditions
t	thickness
ρ	density

Subscripts:

a	aluminum main wall
B	bumper
max	maximum
mw	main wall
pB	penetrated bumper material
pmw	penetrated main wall material
t	total for penetrated portion of bumper and main wall
T	total for complete bumper and main wall
x	general main wall material

APPARATUS AND TEST TECHNIQUE

Projectiles, Bumpers, and Main Walls

The projectiles were all 1.59-mm-diameter spheres of 2024-T4 aluminum alloy with a 0.025-mm tolerance for the diameter and a sphericity of 0.013 mm.

The seven materials tested as bumpers and the density of each material were as follows:

Material	Density, kg/m^3
Aluminum alloy, 2024-T3	2770
Beryllium alloy, hot pressed	1840
Lead	11340
Magnesium alloy, AZ31B-O	1770
Mylar	1390
Neoprene, 40 durometer hardness	1400
Stainless steel, 347 annealed	8030

All densities listed are handbook values. Bumper thicknesses varied from 0.025 mm to 6.35 mm, with a 0.003-mm tolerance for thicknesses less than 0.79 mm and a 0.03-mm tolerance for thicknesses of 0.79 mm and larger. The bumpers tested were generally 7.5 cm wide and 15 cm high; however, the beryllium bumpers were only 5.1 cm by 5.1 cm. The bumpers were rigidly fixed to the main wall and separated from the main wall by a distance of 51 mm. A sketch defining the test configuration is shown in figure 1.

The main walls used in the bumper-protected main wall configuration were all 2024-T4 aluminum alloy. The main walls were nominally 7.5 cm wide, 15 cm high, and 25.4 mm thick. The 25.4-mm thickness was great enough to be considered quasi-infinite, inasmuch as none of the aluminum main walls were penetrated to a depth greater than 5.08 mm or 20 percent of the main wall thickness. It was shown in reference 3 that a wall which is penetrated less than 20 percent by a high-velocity projectile receives the same penetration damage that an infinite wall of the same material would have under the same impact conditions. Unprotected (i.e., no bumpers) quasi-infinite main walls of 2024-T3 aluminum alloy, lead, AZ31B-O magnesium alloy, and annealed 347 stainless steel were also tested.

Projectile Launching Technique

Impact velocities less than 2.4 km/s were obtained with a 5.58-mm rifle. The rifle was fired in open air. The test specimen was located 0.915 m from the muzzle, and was at room temperature and pressure. Impact velocities between 2.4 and 4.3 km/s were obtained with the shock compressed light-gas gun described in reference 4, whereas those greater than 4.3 km/s were obtained with an accelerated reservoir light-gas gun essentially the same as that described in reference 5. The test specimen was enclosed in a vacuum chamber for the light-gas

gun firings and was located 4.58 m from the muzzle of the gun. The pressure in the test chamber was 130 to 270 N/m^2 and the temperature was 290° to 300° K.

Each 1.59-mm-diameter spherical projectile was mounted on a cylindrical nylon sabot, 5.58 mm in diameter and 2.79 mm long. When the sabot left the launch tube, its edge struck a steel bar deflector. The small spherical projectile continued along the flight path while the sabot was deflected and hence separated from the projectile.

Velocity Measuring Technique

The velocity of the projectiles was determined by placing two sheets of Mylar, aluminized on both sides, along the flight path at a known distance apart. The total thickness of the Mylar and aluminum coatings was 6.35 μm. A potential was applied between the aluminum coatings on the opposite sides of each sheet. When the projectile penetrated the first sheet, the aluminum was ionized by the impact and momentarily formed a conducting path between the two aluminum surfaces of the same sheet. The resulting current flow started an electronic time-interval counter. A similar pulse from the second sheet stopped the counter. The distance between sheets and the time of flight between sheets were each measured to an accuracy better than 1 percent. This measured velocity was considered equal to the impact velocity with the deceleration due to drag neglected. Although the drag was negligible for the firings in the evacuated test chamber, it may have slowed the projectiles slightly in the firings in open air in which the aluminized Mylar sheets were 0.661 and 0.814 m from the muzzle and the test specimen was positioned 0.915 m from the muzzle.

Penetration Measuring Technique

Penetrations into the bumpers that were not completely penetrated and into the main walls were measured from the original surface of the undisturbed material to the deepest point in the crater formed by the projectile impact. The penetration into a completely penetrated bumper was considered equal to the bumper thickness. Penetration depths were measured with a depth gage which was tapered from a 0.80-mm-diameter stem to a 0.13-mm-diameter point over a 2.69-mm length. The instrument was accurate to ±0.03 mm; however, penetration measurements by different experienced persons often differed by ±0.06 mm for the deeper penetrations.

PRESENTATION OF RESULTS

Because it is important in space vehicle design to keep the mass of meteoroid protection to a minimum and because materials of different densities were tested as bumpers, the effectiveness of the bumpers was compared on a mass basis rather than on the basis of percentage reduction in total penetration. The total penetration depth is defined as the penetration into the bumper plus the

penetration into the main wall in the case of a bumper-protected main wall, and merely the penetration into the main wall in the case of an unprotected main wall.

The parameter m_t is the total mass per unit area of penetrated material and is hereinafter referred to as the total penetration damage. The parameter m_t is defined by the equation

$$m_t = m_{pB} + m_{pmw} = P_B\rho_B + P_{mw}\rho_{mw} \tag{1}$$

When the projectile is unable to penetrate the bumper completely, the term $P_{mw}\rho_{mw}$ is zero. When the bumper is completely penetrated, the term $P_B\rho_B$ becomes $t_B\rho_B$. When no bumper is used, the term $P_B\rho_B$ is, of course, zero. The difference between the value of m_t for an unprotected aluminum target and that for a bumper-protected target is considered to be a measure of the effectiveness of the bumper.

The relative effectiveness of different bumpers was determined by comparing the maximum total penetration damage $m_{t,max}$ that each permitted in the 0 to 4.9 km/s velocity range. The smaller the value of $m_{t,max}$, the more effective the bumper.

Penetration into Unprotected Quasi-Infinite Main Walls

The total penetration damage m_t for unprotected quasi-infinite main walls of various materials is shown in figure 2 as a function of the impact velocity. An increase in the impact velocity resulted in an increase in the total penetration damage m_t through the entire range investigated for each material, except for the lead in the 1.9 to 2.7 km/s range. This range was the transition region from undeformed projectile to fluid impact reported in reference 6. The total penetration damage for the aluminum and magnesium main walls was small compared with the damage for stainless-steel and lead main walls. The data used to construct the curves for lead, stainless-steel, aluminum, and magnesium are presented in table I. Thick beryllium plates suitable for quasi-infinite main walls were not available for these tests. However, during the tests of bumper-protected main walls discussed subsequently, beryllium was used as a bumper material. In two of the tests the penetration into the bumper was less than 20 percent of the bumper thickness (see table II). Thus, in these two tests the bumpers were acting as quasi-infinite walls and these data are shown in figure 2. Beryllium bumpers acting as quasi-infinite main walls received little penetration damage compared with the damage for stainless-steel and lead main walls. Also shown in figure 2 are data from four tests where the beryllium bumpers were partially penetrated to a depth greater than 20 percent of the bumper thickness. Because the bumpers were not acting as quasi-infinite walls in these tests, each of the four data points is marked with an arrow pointing down to indicate that the total penetration damage for a quasi-infinite beryllium wall would be lower than that shown. A straight line was faired through the beryllium data points, with the most emphasis being placed on the two points

for quasi-infinite walls and with the line falling below the points for the finite-thickness walls.

Penetration into Bumper-Protected Main Walls

The total penetration damage m_t produced in the various bumper-protected targets investigated is presented in figures 3 to 9 as a function of the impact velocity. Each of the figures is for a different bumper material and each figure presents data for three bumper thicknesses. The main wall material was always aluminum. In general, the (b) part of each figure represents the most effective bumper thickness tested for the material under consideration. The (a) and (c) parts, in general, represent bumper thicknesses less than and larger than the optimum thickness, respectively. Exceptions occur in figures 7 and 8 because of the limitation of thicknesses available for Mylar and neoprene. Additional curves were obtained for other thicknesses than those presented in the figures in order to accurately establish the most effective bumper thickness. Figure 3 is discussed in detail whereas figures 4 to 9 are discussed more briefly because of the many similarities that exist in the behavior of bumpers of different materials. The data from which these curves and the additional curves mentioned were constructed are presented in table II.

DISCUSSION OF RESULTS

Effect of Bumper Thickness

The total penetration damage m_t for 2024-T3 aluminum-alloy bumpers of three different thicknesses is shown in figure 3 as a function of the impact velocity. The horizontal dashed line shows the mass per unit area of the bumper. The diagonal dashed line represents the damage that would be created in an unprotected quasi-infinite aluminum main wall and was taken from figure 2.

The results for a 0.025-mm-thick bumper are presented in figure 3(a). The total penetration damage increased when the impact velocity was increased up to approximately 5.48 km/s. A further increase in the impact velocity to 5.88 km/s resulted in decreased total penetration damage. The maximum total penetration damage $m_{t,max}$ was approximately 7.0 kg/m^2. This bumper was not very effective in reducing total penetration damage at velocities less than 5.48 km/s; that is, the total penetration damage was not much different from that for an unprotected aluminum main wall at those velocities. The effectiveness of the bumper at the higher impact velocity was due to the fragmentation of the projectile as it penetrated the bumper at that velocity. The fragmented projectile produced a number of small, shallow craters in the main wall instead of the one large, deep crater as was produced at the lower velocities.

The behavior of the 0.41-mm-thick bumper in figure 3(b) was similar to that of the 0.025-mm-thick bumper in figure 3(a). However, the thicker bumper was more effective at all velocities greater than 3 km/s. The maximum total

penetration damage $m_{t,max}$ of 4.0 kg/m^2 is less than the maximum penetration in figure 3(a).

The behavior of an excessively thick bumper is illustrated in figure 3(c). Impact velocities of 4.40 km/s were required for the projectile to penetrate the bumper. At all velocities less than 4.40 km/s, the bumper was ineffective in reducing total penetration damage; in fact, the bumper enhanced damage by increasing the damage to the bumper while the main wall remained undamaged. At all velocities greater than 4.40 km/s this bumper was less effective than the bumpers in figures 3(a) and 3(b), because the total penetration damage of 8.81 kg/m^2 required to penetrate this bumper is greater than the maximum total penetration damage in figures 3(a) and 3(b).

The most effective of the bumpers tested was the 0.41-mm-thick bumper which permitted a maximum total penetration of 4.0 kg/m^2. The data in figure 3 illustrate the existence of an optimum bumper thickness, a fact previously established in reference 2. Both thicker and thinner bumpers permit greater values of maximum total penetration damage, the thinner because a greater impact velocity is required to cause projectile fragmentation, the thicker because the penetration damage to the bumper itself must be extensive.

Effect of Bumper Material

The beryllium, lead, magnesium, Mylar, neoprene, and stainless-steel bumpers behaved much like the aluminum bumpers. (See figs. 3 to 9.) In general, the total penetration damage m_t increased as the impact velocity increased to a maximum value at the velocity required for projectile fragmentation and decreased with further increases in the impact velocity. It should be noted that in figures 3(b), 4(b), 5(b), 6(b), and 9(b), which present data for the optimum thicknesses for the various bumper materials, the values of bumper mass per unit area m_B are all approximately the same. This fact suggests that even though the optimum bumper thicknesses varied from 0.13 mm to 0.81 mm for the various materials, there may be an optimum value of mass per unit area independent of material. In order to examine this possibility further, the maximum total penetration damage $m_{t,max}$ for the various bumper materials tested was plotted as a function of the mass per unit area of the bumper m_B not only for the optimum bumpers but for all bumpers tested in which the total penetration damage increased to a maximum value and decreased with further increases in impact velocity. The results are shown in figure 10. Data points in this figure were all obtained from the data in table II. The dashed line represents $m_{t,max} = m_B$. The difference between the dashed curve and the data curve is maximum penetration damage produced in the main wall. The figure shows that the maximum penetration damage to the main wall continually decreased with increased bumper mass per unit area and became almost negligible when the bumper mass per unit area was greater than about 15 kg/m^2. However, the maximum total penetration damage, a more significant quantity, was a minimum when the bumper mass per unit area was between 0.5 and 1.5 kg/m^2; therefore, the optimum bumper mass per unit area is in that range. Particularly significant is the good agreement between data for different bumper materials. This agreement indicates

that whereas the maximum total penetration depends on the mass per unit area of the bumper, it is affected very little by the choice of bumper material.

Many of the beryllium bumpers tested developed cracks which ran from the point of impact to the edge of the 5.1- by 5.1-cm bumper. There was also a tendency for a spallation cavity to be produced on the back side of the beryllium bumpers opposite the point of impact when the bumper was only partially penetrated. The penetration damage in the thick beryllium bumper (fig. 4(c)) was a measure of the damage occurring on the front side only; that is, the spallation cavity was neglected. Therefore the penetration damage increased slowly with increased impact velocity until the bottoms of the impact crater and spallation cavity met. The unusual curve in figure 4(c) is due to the spallation phenomenon. At the velocity at which the impact crater and spallation cavity met, the penetration damage to the bumper abruptly increased. Both the spallation and cracking can be seen in figure 11, where photographs of the front and back side of one of the beryllium bumpers tested are presented.

Lead bumpers of the three thicknesses considered in figure 5 were so easily penetrated that no data on partial penetration were obtained. Data for thicker lead bumpers appear in table II and show that a 1.57-mm-thick lead bumper was completely penetrated at 1.04 km/s, the lowest impact velocity obtained. No partial penetration data were obtained for Mylar either, inasmuch as only thin Mylar bumpers were available. Because it was not possible to define the optimum bumper mass for Mylar with the available bumpers, only two curves are presented in figure 7. The maximum total penetration damage produced in the 0.25-mm-thick bumper (see fig. 7(b)) did agree well with that obtained for other bumpers of the same mass per unit area but of different materials (see fig. 10). The holes left in the neoprene bumpers, particularly the thicker neoprene bumpers, were smaller than those in the bumpers made of other materials. The thick neoprene bumpers tended to close up around the hole and make it appear smaller than projectile size. Unusually extensive damage was produced in the main walls protected by the 0.81-mm-thick stainless-steel bumpers. The projectile was fragmented during penetration of the bumper and did little damage to the main wall. The extensive damage was caused by large fragments of the stainless-steel bumper. Thus, it was the bumper fragments, and not the projectile, which controlled the total penetration damage. Apparently the choice of a bumper material from materials which are dense compared with the projectile must be made with care. Dense materials like stainless steel which create relatively large fragments while being penetrated should be avoided in favor of materials like lead which create relatively small fragments.

Effect of Main Wall Material

Quasi-infinite main walls.- The penetration damage that would have occurred in the tests described graphically in figures 3 to 10, if quasi-infinite beryllium, lead, magnesium, or stainless steel had been used for the main wall material rather than aluminum, can be calculated with the use of figure 2 provided one assumption is made. At a given impact velocity the fragments striking the bumper-protected quasi-infinite aluminum, beryllium, lead, magnesium, and stainless-steel main walls must be assumed to produce penetration damage in the same ratio as that indicated in figure 2, which shows the penetration produced

by aluminum projectiles impacting unprotected main walls of these same materials. With this assumption, the total penetration damage that would occur if the main wall were some material other than aluminum is given by the equation

$$m_{t,x} = R_x(m_{t,a} - m_B) + m_B \qquad (m_{t,a} \geqq m_B) \qquad (2)$$

where $m_{t,a}$ is the total penetration damage that occurred when the main wall was aluminum, as in figures 3 to 10, and where R_x is the ratio of the penetration damage in the main wall being considered to that in the aluminum wall at the velocity with which the most damaging fragment struck the main wall. The ratio R_x was determined from figure 2. When the curves in figure 2 are straight lines through the origin, as they are for aluminum, beryllium, magnesium, and stainless steel, R_x is independent of the velocity of the most damaging fragment and the necessity for determining that velocity is eliminated. For those materials, R_x is equal to the ratio of the slope of the curve for the material being considered to the slope of the curve for aluminum. In order to simplify the calculation of R_x for lead, the curve for lead was approximated by a straight line through the origin and faired through the three highest velocity data points. The values of R_x obtained were 0.37 for beryllium, 1.0 for magnesium, 1.5 for stainless steel, and 5.4 for lead.

Finite-thickness main walls.- The quasi-infinite main walls used in all the tests described in this report are impractical for spacecraft design. If the data could be converted to give the total mass per unit area of bumper and finite-thickness main wall required to just defeat the projectile, it would be of practical interest. Previous investigations show that for a given material at a given impact velocity the finite-thickness wall required to defeat a particle can be determined by multiplying the penetration depth produced by that particle in a quasi-infinite wall by a factor F. (See, for example, ref. 3.) The value of this factor is very often taken to be 1.5.

A series of tests were reported in reference 7 in which bumpers and finite-thickness main walls with a standoff distance of 12 projectile diameters were struck by projectiles traveling 6.1 km/s. The main walls were thick enough to prevent particle penetration and no total penetrations of the main walls were observed. However, in many cases a spallation cavity was created on the back side of the main wall opposite the area where the many projectile and bumper fragments struck the main wall. This spallation cavity was caused by the reflection of a strong pressure pulse created by the collective impacts of the many fragments. It is possible, at high impact velocities, for the spallation cavity to be deep enough to meet the crater bottoms, in which case the main wall would be completely penetrated. Spallation can also be accompanied by cracking or rupturing of the main wall. Reference 7 shows that the spallation cavity could be reduced in depth or even eliminated for the aforementioned velocity and standoff distance by using a dense material for the bumper, without changing the mass per unit area of the bumper. Inasmuch as the penetration damage was affected very little by the bumper material, this difference observed in the spallation which occurred when thin main walls were used should be considered when choosing a bumper material.

Pressure-pulse failures, that is, spallation, cracking, and rupturing, can be eliminated by using a large standoff distance. When the standoff distance is large, the fragments impact over a large area of the main wall and the energy received per unit area is less than that required for pressure-pulse failure. Reference 8 shows that the standoff distance required to prevent pressure-pulse failure of the main wall is a function of the impact velocity. Very large standoff distances may be required to prevent pressure-pulse failures at maximum meteoroid velocities.

If the pressure-pulse failures are neglected, that is, if sufficiently large standoff distances are used, the total mass required to defeat the aluminum projectiles can be calculated by using the data in figure 10 and the appropriate conversion factor F from quasi-infinite to maximum finite wall penetration. The data in figure 10 apply at any large standoff distance because the maximum total penetration damage is caused by an intact projectile and is therefore independent of the standoff distance. There are adequate data in this report to calculate approximately the value of F for aluminum, beryllium, magnesium, and stainless-steel targets by the method in reference 3. The values calculated from the data in this report are 1.3 to 1.4 for aluminum, 3.8 to 4.0 for beryllium, 1.4 to 1.6 for magnesium, and 2.2 to 2.3 for stainless steel. A value of 1.5 is assumed for lead since there are no data in this report that can be used to determine the value. The total mass of bumper and finite-thickness main wall required to defeat the 1.59-mm-diameter aluminum projectiles at the velocity of maximum total penetration damage can then be calculated. The calculated total mass is more than sufficient to defeat the projectile at any other velocity in the range considered in figure 10. The total mass required when an aluminum main wall is used can be calculated by using the equation

$$\left(m_{T,max}\right)_a = F_a\left[\left(m_{t,max}\right)_a - m_B\right] + m_B \tag{3}$$

where $\left(m_{T,max}\right)_a$ is the total mass required, F_a is the appropriate conversion factor from quasi-infinite to finite-thickness main walls for aluminum, and $\left(m_{t,max}\right)_a$ and m_B are the coordinates in figure 10. The total mass required when the finite main wall is a material other than aluminum can be calculated by using the equation

$$\left(m_{T,max}\right)_x = F_x R_x\left[\left(m_{t,max}\right)_a - m_B\right] + m_B \tag{4}$$

where F_x is the conversion factor from quasi-infinite to finite-thickness main walls for the material being considered. The calculated results obtained by using equation (4) appear in figure 12, where the curves are independent of the bumper material. The figure shows that the optimum bumper mass is a function of the main wall material. The main wall material can greatly affect the effectiveness of a bumper and main wall configuration, the less dense material generally being more effective. The optimum bumper mass is approximately

1 kg/m^2 when the main wall is aluminum, whereas a bumper mass of approximately 3 kg/m^2 is optimum when a lead main wall is used. The curve for beryllium is dashed because the beryllium bumpers tested were found to be particularly susceptible to spalling and cracking, the type of damage caused by a pressure pulse. They usually developed cracks and a large spallation cavity when they were partially penetrated. There is, therefore, some question as to whether the beryllium main walls, indicated as adequate in figure 12, can withstand the pressure pulse generated even at large standoff distances. The diagonal dashed line labeled $m_{T,max} = m_B$ represents the part of the total mass which is in the bumper. The difference between this curve and the data curves is the part of the total mass which is in the main wall.

The curves in figures 3 to 9 show that, in general, the penetration damage decreases with increased impact velocity for velocities greater than the velocity required to fragment the projectile. If this trend continues to maximum meteoroid velocities, the maximum total penetration damage observed at a low impact velocity would be the absolute maximum total penetration damage obtainable for projectiles traveling at meteoroid velocities. If this trend does continue to maximum meteoroid velocities, the mass required to defeat the aluminum projectiles in the zero to 4.9 km/s range, as given in figure 12, would be all that is required to defeat these projectiles at any meteoroid velocity. Of course, the assumption is made that the standoff distance is large enough to prevent failure by spallation, cracking, or rupturing, a danger that becomes more severe as the impact velocity is increased.

CONCLUSIONS

The results of an investigation to determine the relative effectiveness of aluminum, beryllium, lead, magnesium, Mylar, neoprene, and stainless-steel bumpers and the relative effectiveness of aluminum, beryllium, lead, magnesium, and stainless-steel main walls in reducing the penetration damage produced by 1.59-mm-diameter aluminum projectiles at velocities up to 5.88 km/s have led to the following conclusions:

1. In the velocity range of the investigation, bumper thicknesses which were effective in reducing total penetration damage were found for all of the bumper materials tested.

2. The protection provided by a bumper to a quasi-infinite main wall was dependent on the mass per unit area of the bumper and was affected very little by the bumper material. Previous investigations have indicated that dense materials were desirable when a thin main wall was used because the amount of spallation was decreased. However, the choice of a bumper material from materials which are dense compared with the projectile material must be made with care to avoid the creation of bumper fragments which are more damaging to the main wall than projectile fragments.

3. The main wall material can greatly affect the effectiveness of a bumper and main wall configuration, the less dense materials generally being more effective.

4. The optimum bumper mass was independent of the bumper material but was dependent on the main wall material. The optimum bumper mass varied from 1 kg/m^2 when a finite aluminum main wall was used to 3 kg/m^2 when a finite lead main wall was used.

5. The total penetration damage for unprotected aluminum and magnesium main walls was small compared with the damage for stainless-steel and lead main walls. Beryllium bumpers acting as quasi-infinite main walls also received little penetration damage. However, it is doubtful if finite thickness beryllium could be used as a main wall because the finite beryllium bumpers tested usually developed cracks and a large spallation cavity when they were partially penetrated.

Langley Research Center,
National Aeronautics and Space Administration,
Langley Station, Hampton, Va., August 10, 1965.

REFERENCES

1. Whipple, Fred L.: Meteoritic Phenomena and Meteorites. Physics and Medicine of the Upper Atmosphere, Clayton S. White and Otis O. Benson, Jr., eds., The Univ. of New Mexico Press (Albuquerque), 1952, pp. 137-170.

2. Humes, Donald H.: An Experimental Investigation of the Effectiveness of Single Aluminum Meteoroid Bumpers. NASA TN D-1784, 1963.

3. Kinard, William H.; Lambert, C. H., Jr.; Schryer, David R.; and Casey, Francis W., Jr.: Effect of Target Thickness on Cratering and Penetration of Projectiles Impacting at Velocities to 13,000 Feet Per Second. NASA MEMO 10-18-58L, 1958.

4. Collins, Rufus D., Jr.; and Kinard, William H.: The Dependency of Penetration on the Momentum Per Unit Area of the Impacting Projectile and the Resistance of Materials to Penetration. NASA TN D-238, 1960.

5. Curtis, John S.: An Accelerated Reservoir Light-Gas Gun. NASA TN D-1144, 1962.

6. Summers, James L.: Investigation of High-Speed Impact: Regions of Impact and Impact at Oblique Angles. NASA TN D-94, 1959.

7. Maiden, C. J.: Investigation of Fundamental Mechanism of Damage to Thin Targets by Hypervelocity Projectiles. TM 63-201 (Contract No. Nonr 3891(00)(x)), GM Defense Res. Lab., Gen. Motors Corp., Mar. 1963.

8. Nysmith, C. Robert; and Summers, James L.: An Experimental Investigation of the Impact Resistance of Double-Sheet Structures at Velocities to 24,000 Feet Per Second. NASA TN D-1431, 1962.

TABLE I.- IMPACT DATA FOR 1.59-MM-DIAMETER ALUMINUM SPHERES

STRIKING UNPROTECTED QUASI-INFINITE TARGETS

Impact velocity, km/s	Total penetration, mm
Aluminum-alloy target	
0.13	0.20
.23	.20
.58	.41
1.19	.51
1.55	.76
1.62	.76
2.83	1.42
2.93	1.63
3.14	1.88
3.44	1.85
3.47	1.70
3.60	1.88
3.60	1.93
3.63	1.98
3.81	2.03
3.87	1.96
3.96	2.06
4.05	2.21
5.12	2.49
Lead target	
0.61	1.12
1.52	1.70
1.92	1.88
2.62	1.93
3.29	2.39
4.24	2.79
Magnesium-alloy target	
0.76	0.81
1.40	1.52
1.62	1.85
1.71	2.03
1.92	2.26
2.87	2.59
3.38	2.97
3.74	3.25
3.96	3.23
Stainless-steel target	
0.82	0.15
1.22	.28
1.46	.36
1.68	.36
1.89	.51
2.19	.64
2.71	.79
3.69	1.04
3.84	1.07
3.87	.99
4.42	1.17
4.57	1.02

TABLE II.- IMPACT DATA FOR 1.59-MM-DIAMETER ALUMINUM SPHERES STRIKING QUASI-INFINITE ALUMINUM MAIN WALLS PROTECTED BY SINGLE BUMPER WITH 51-MM STANDOFF DISTANCE

Impact velocity, km/s	Total penetration, mm
Aluminum bumper; t_B = 0.025 mm	
1.01	0.51
1.92	1.07
3.57	1.60
3.96	1.85
4.11	1.80
4.42	2.01
4.75	2.29
5.43	2.51
5.88	1.85
Aluminum bumper; t_B = 0.41 mm	
0.40	0.41
1.07	.53
1.46	.66
1.65	.89
1.77	.94
2.44	.94
2.96	1.50
3.32	1.09
3.32	1.47
3.57	1.17
4.51	1.12
5.24	.94
Aluminum bumper; t_B = 0.81 mm	
0.49	0.05
1.10	.86
1.80	.97
2.04	1.07
2.74	1.52
3.35	1.80
3.54	1.40
3.69	1.32
4.36	1.63
5.09	1.22
Aluminum bumper; t_B = 1.57 mm	
0.52	0.13
1.80	1.83
2.16	1.80
2.50	1.75
2.80	1.65
3.23	1.75
3.57	2.16
3.75	1.85

Impact velocity, km/s	Total penetration, mm
Aluminum bumper; t_B = 3.18 mm	
0.46	0.23
.61	.13
1.34	.69
1.80	.97
1.86	1.17
2.26	1.68
2.65	1.75
3.75	2.54
4.39	3.23
Beryllium bumper; t_B = 0.41 mm	
2.47	1.32
3.29	1.19
3.60	1.45
4.30	1.14
Beryllium bumper; t_B = 0.69 mm	
2.68	1.35
3.11	1.40
4.08	1.42
Beryllium bumper; t_B = 1.75 mm	
2.19	1.75
*2.71	1.91
3.38	1.96
4.39	2.24
5.00	2.03
Beryllium bumper; t_B = 3.38 mm	
1.52	0.46
2.65	1.02
3.57	3.43
4.63	3.56
Beryllium bumper; t_B = 5.21 mm	
2.35	0.94
3.57	1.96
3.93	1.88
†4.24	2.03

*t_B = 1.65 mm for this test run.
†t_B = 4.83 mm for this test run.

TABLE II.- IMPACT DATA FOR 1.59-MM-DIAMETER ALUMINUM SPHERES STRIKING QUASI-INFINITE ALUMINUM MAIN WALLS PROTECTED BY SINGLE BUMPER WITH 51-MM STANDOFF DISTANCE - Continued

Impact velocity, km/s	Total penetration, mm
Lead bumper; t_B = 0.025 mm	
1.04	0.43
1.46	.66
1.92	1.02
2.62	1.22
3.72	1.70
3.96	1.17
4.00	1.02
Lead bumper; t_B = 0.13 mm	
1.77	0.64
2.04	.64
2.68	.97
2.80	.81
2.83	.84
2.96	.84
3.38	.76
3.60	.74
3.75	.91
3.78	.84
4.02	.74
4.15	.81
Lead bumper; t_B = 0.41 mm	
1.01	0.46
1.55	.53
1.80	.61
1.98	.56
2.99	.79
3.17	.64
3.90	.74
4.36	.64
4.54	.66
4.79	.56
Lead bumper; t_B = 0.89 mm	
0.79	0.89
1.04	.89
1.22	.89
1.49	.89
1.80	.89
2.71	1.24
2.77	1.17
3.14	1.04
3.51	1.09
3.66	1.02
3.75	.99
4.27	.97
5.09	.97
Lead bumper; t_B = 1.57 mm	
1.04	1.57
1.28	1.57
1.55	1.57
1.80	1.57
2.10	1.57
2.19	1.78
2.77	1.57
3.32	1.78
3.47	1.75
4.11	1.60

Impact velocity, km/s	Total penetration, mm
Magnesium bumper; t_B = 0.05 mm	
1.34	0.69
2.04	1.12
2.41	1.17
2.87	1.32
3.20	1.63
3.51	1.70
4.18	1.96
4.21	2.03
4.54	1.70
Magnesium bumper; t_B = 0.41 mm	
1.04	0.74
1.40	.97
1.65	1.07
2.04	1.17
2.26	1.14
2.83	1.30
2.99	1.47
3.35	1.17
3.78	1.27
4.15	1.19
Magnesium bumper; t_B = 0.81 mm	
0.85	0.86
1.16	1.04
1.19	.99
1.52	.94
1.83	1.52
2.01	1.27
2.56	1.60
2.80	1.24
2.90	1.57
3.20	1.37
3.38	1.37
3.54	1.52
4.02	1.63
4.11	1.55
4.18	1.55
Magnesium bumper; t_B = 1.57 mm	
0.52	0.36
.55	.38
.76	.71
1.40	1.60
1.49	1.60
1.74	1.63
2.04	1.65
2.10	1.75
2.35	1.85
3.29	1.96
3.78	2.24
5.33	1.96
Magnesium bumper; t_B = 3.18 mm	
0.67	0.58
1.19	1.17
1.80	2.16
2.07	2.21
2.53	3.18
2.90	3.18
2.99	3.18
3.44	3.28
3.44	3.18
3.69	3.30
5.36	3.38

TABLE II.- IMPACT DATA FOR 1.59-MM-DIAMETER ALUMINUM SPHERES STRIKING QUASI-INFINITE ALUMINUM MAIN WALLS PROTECTED BY SINGLE BUMPER WITH 51-MM STANDOFF DISTANCE - Continued

Impact velocity, km/s	Total penetration, mm
Mylar bumper; t_B = 0.025 mm	
0.67	0.69
1.43	.79
1.65	.94
1.95	1.07
2.68	1.24
2.96	1.37
3.26	1.73
3.69	1.91
4.02	1.88
Mylar bumper; t_B = 0.13 mm	
0.70	0.43
.98	.51
1.22	.64
1.58	.97
1.89	1.09
2.56	1.40
2.65	1.42
2.93	1.52
3.08	1.70
3.23	1.78
3.35	1.63
3.44	1.91
3.90	1.85
4.27	2.03
Mylar bumper; t_B = 0.25 mm	
0.67	0.41
1.19	.76
1.43	.76
1.62	.89
1.98	1.07
2.71	1.30
2.87	1.47
2.96	1.60
3.66	1.70
3.72	1.70
4.18	1.73
4.39	1.57

Impact velocity, km/s	Total penetration, mm
Neoprene bumper; t_B = 0.41 mm	
1.07	0.81
1.80	1.14
2.50	1.22
2.90	1.42
3.41	1.57
3.72	1.37
4.05	1.32
Neoprene bumper; t_B = 0.81 mm	
0.98	1.07
1.95	1.40
2.65	1.70
3.32	1.68
3.93	1.65
4.24	1.78
Neoprene bumper; t_B = 1.57 mm	
0.98	1.80
1.74	1.85
2.41	2.18
2.99	2.26
3.87	2.21
4.54	2.18
Neoprene bumper; t_B = 3.18 mm	
0.98	3.30
1.92	3.30
2.41	3.28
2.93	3.18
3.05	3.35
3.14	3.18
3.20	3.28
3.38	3.38
4.18	3.35
Neoprene bumper; t_B = 6.35 mm	
0.98	≈2.0
1.83	4.3

TABLE II.- IMPACT DATA FOR 1.59-MM-DIAMETER ALUMINUM SPHERES STRIKING QUASI-INFINITE ALUMINUM MAIN WALLS PROTECTED BY SINGLE BUMPER WITH 51-MM STANDOFF DISTANCE - Concluded

Impact velocity, km/s	Total penetration, mm
Stainless-steel bumper; t_B = 0.025 mm	
1.34	0.38
2.19	1.02
2.90	1.45
3.41	1.68
4.42	1.83
4.82	1.52
Stainless-steel bumper; t_B = 0.13 mm	
0.98	0.43
1.55	.69
1.92	.86
2.80	1.04
2.83	.99
3.14	1.40
3.47	.86
3.66	.89
3.81	.91
3.99	.91
4.24	.86
Stainless-steel bumper; t_B = 0.25 mm	
0.76	0.25
1.07	.38
1.74	.56
1.89	.51
2.53	1.02
3.20	1.14
3.38	.74
3.54	1.07
4.18	.79
Stainless-steel bumper; t_B = 0.41 mm	
0.46	0.28
.49	.36
1.10	.41
1.46	.58
1.86	.46
2.35	1.42
2.50	.89
2.56	1.30
3.20	1.68
3.38	1.04
3.57	1.30
3.69	1.04
3.90	1.04
4.21	1.19
Stainless-steel bumper; t_B = 0.81 mm	
0.58	0.25
.76	.38
1.13	.69
1.40	.99
1.86	.89
2.13	1.04
2.29	1.09
2.65	1.55
2.71	1.19
2.96	1.88
3.05	1.47
3.60	2.16
4.54	1.55
5.43	1.65
Stainless-steel bumper; t_B = 1.57 mm	
0.73	0.03
.85	.25
1.10	.28
1.25	.36
1.49	.48
1.80	.61
2.56	1.17
2.59	1.37
2.71	1.57
2.77	1.57
3.02	1.57
3.66	1.73
3.81	1.83
3.84	1.83
3.99	1.73
4.30	1.93

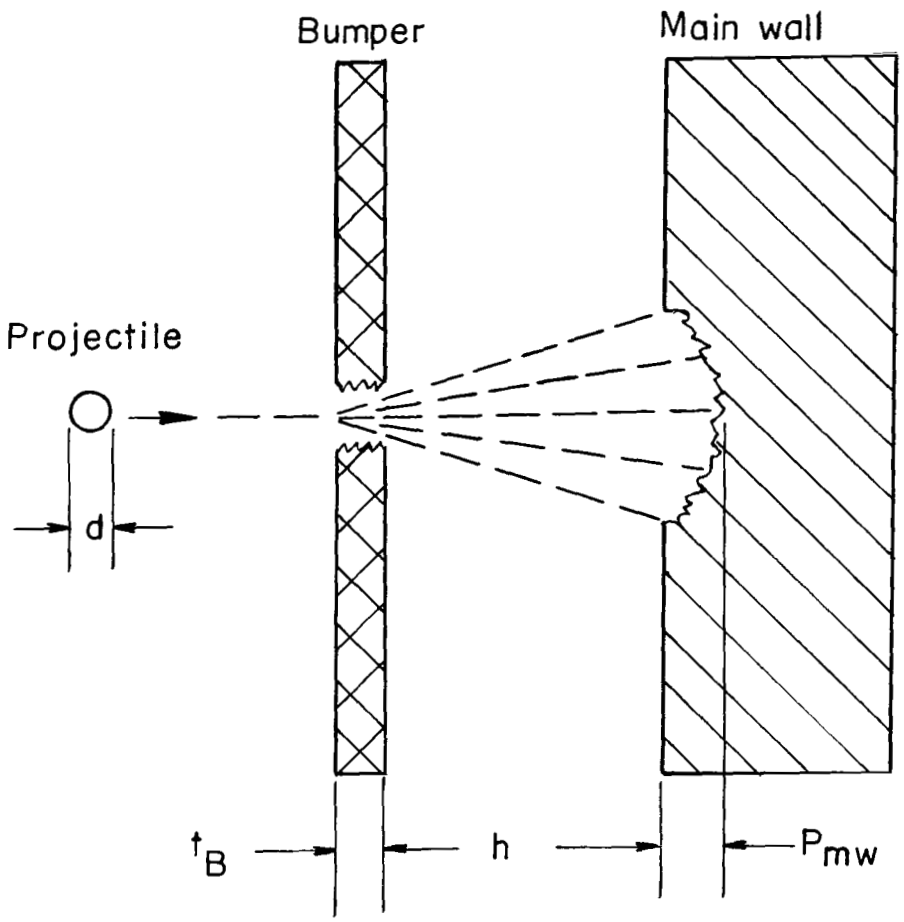

Figure 1.- Bumper-protected main wall configuration.

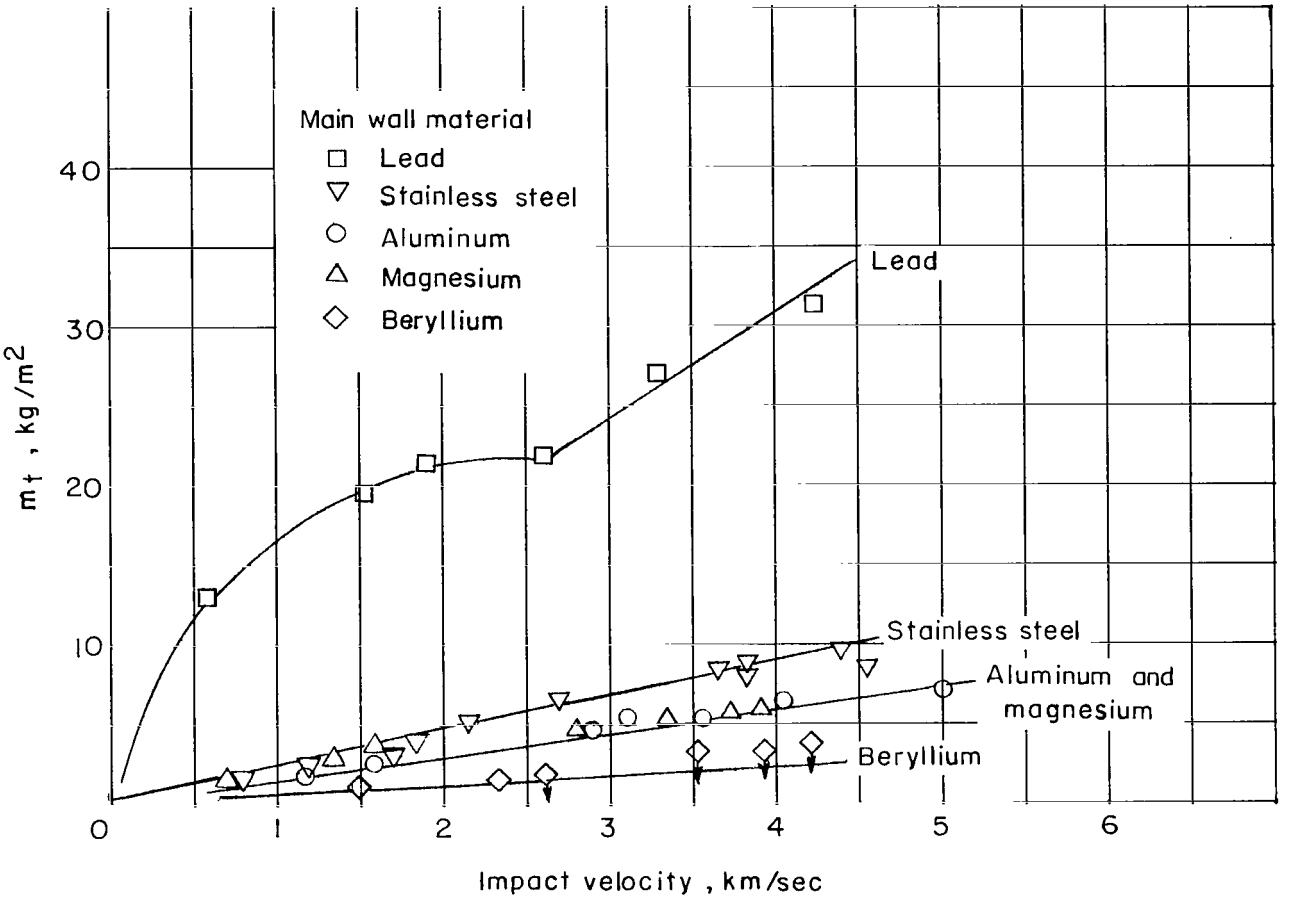

Figure 2.- Effect of main wall material on total penetration damage for an unprotected quasi-infinite main wall. Projectile was 1.59-mm-diameter aluminum sphere.

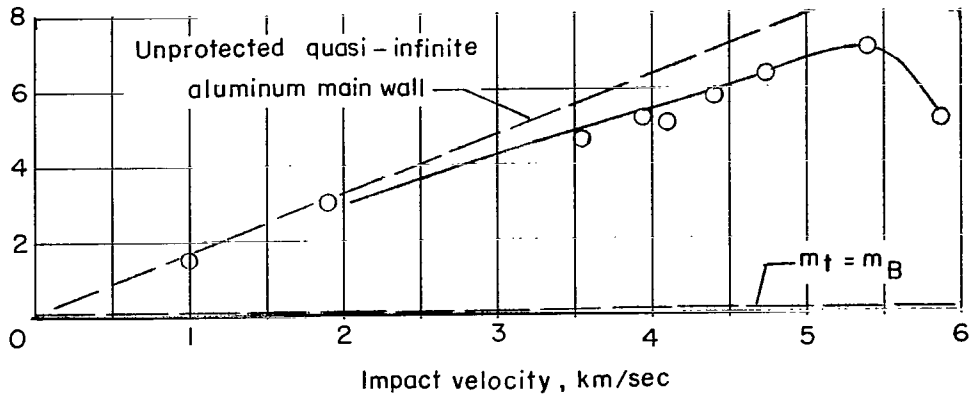

(a) t_B = 0.025 mm; m_B = 0.069 kg/m^2.

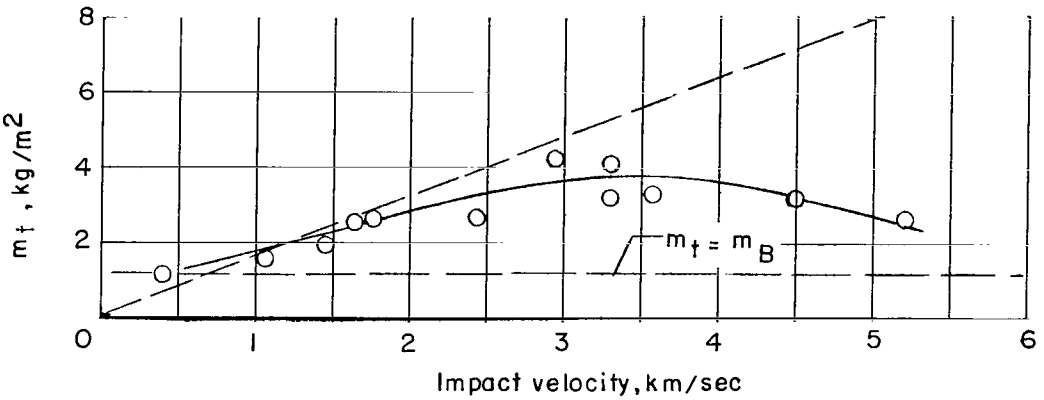

(b) t_B = 0.41 mm; m_B = 1.14 kg/m^2.

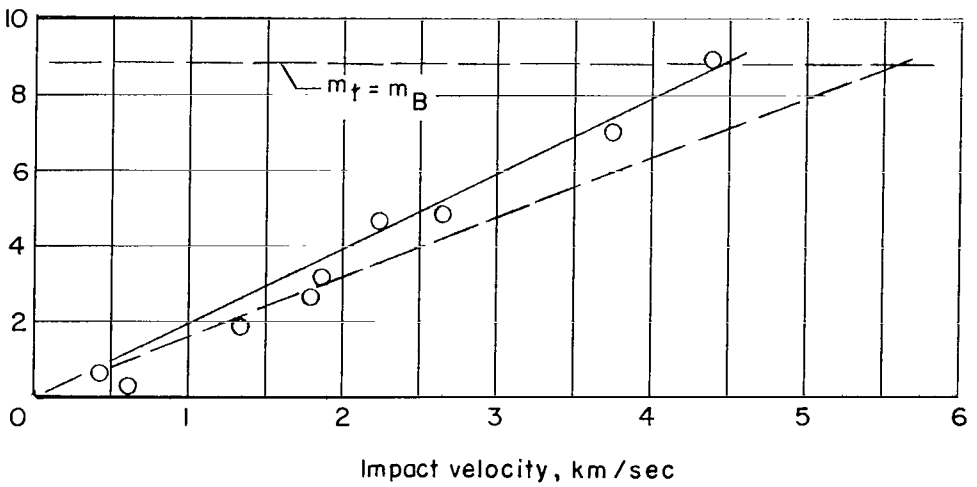

(c) t_B = 3.18 mm; m_B = 8.81 kg/m^2.

Figure 3.- Effect of bumper thickness on total penetration damage. Bumper material was 2024-T3 aluminum alloy; projectile was 1.59-mm-diameter aluminum sphere.

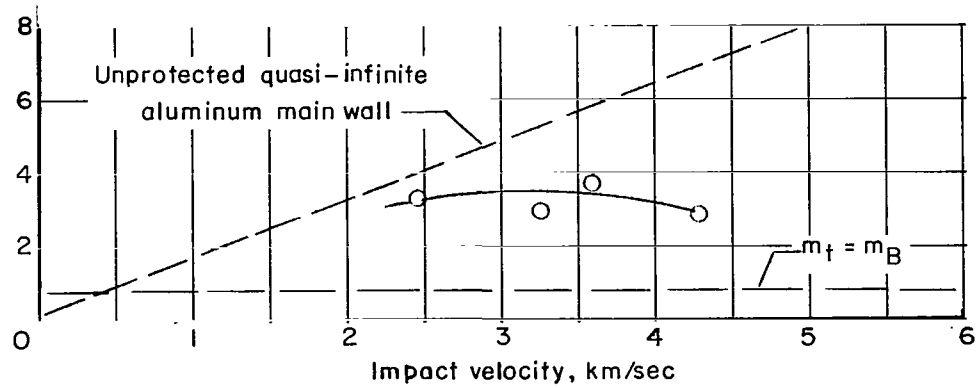

(a) t_B = 0.41 mm; m_B = 0.75 kg/m^2.

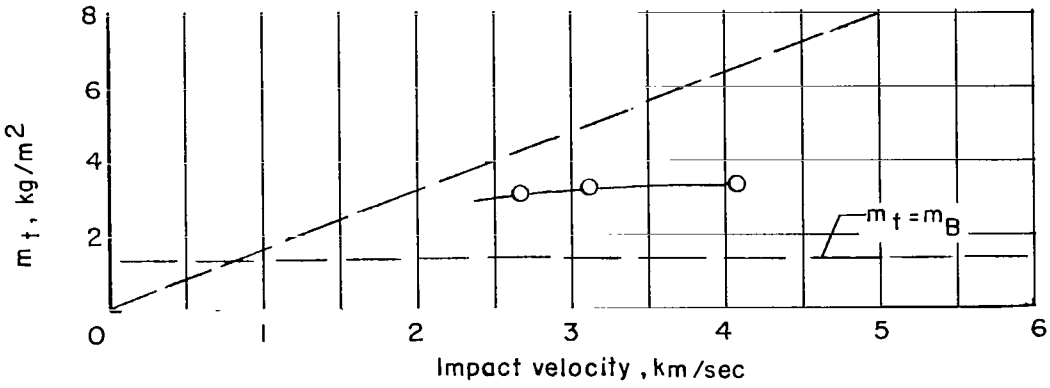

(b) t_B = 0.69 mm; m_B = 1.27 kg/m^2.

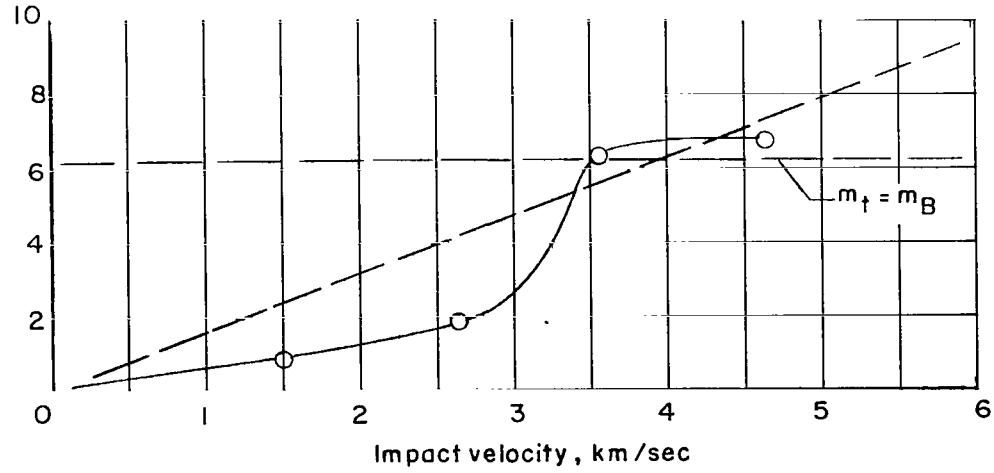

(c) t_B = 3.38 mm; m_B = 6.22 kg/m^2.

Figure 4.- Effect of bumper thickness on total penetration damage. Bumper material was beryllium alloy; projectile was 1.59-mm-diameter aluminum sphere.

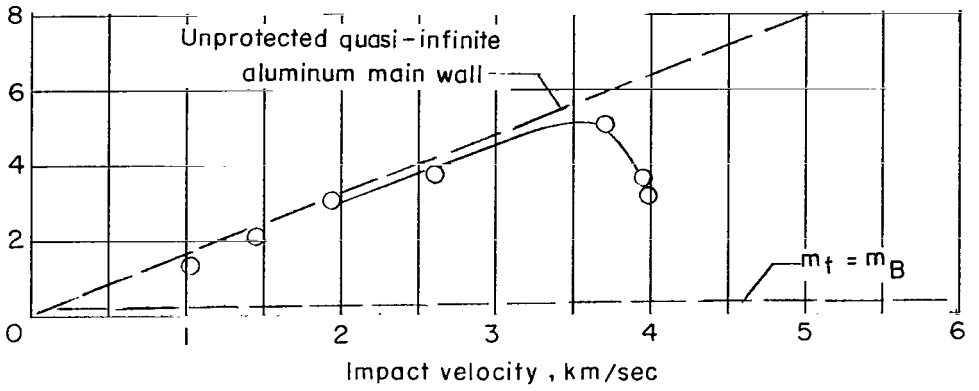

(a) t_B = 0.25 mm; m_B = 0.34 kg/m^2.

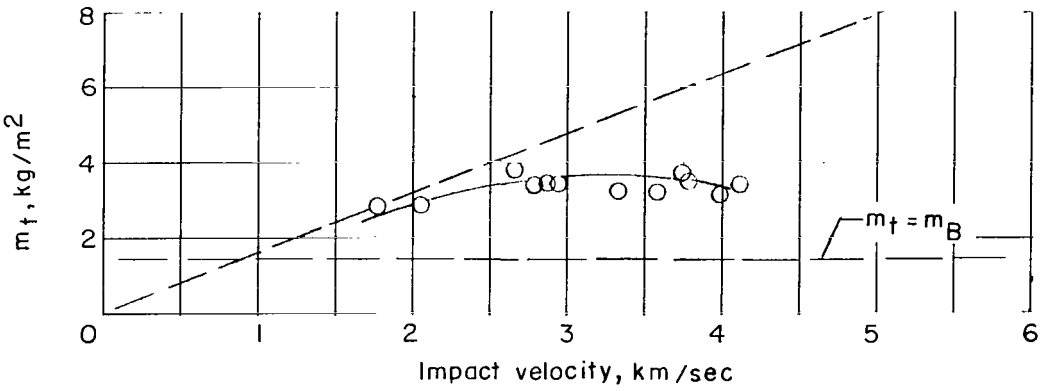

(b) t_B = 0.13 mm; m_B = 1.47 kg/m^2.

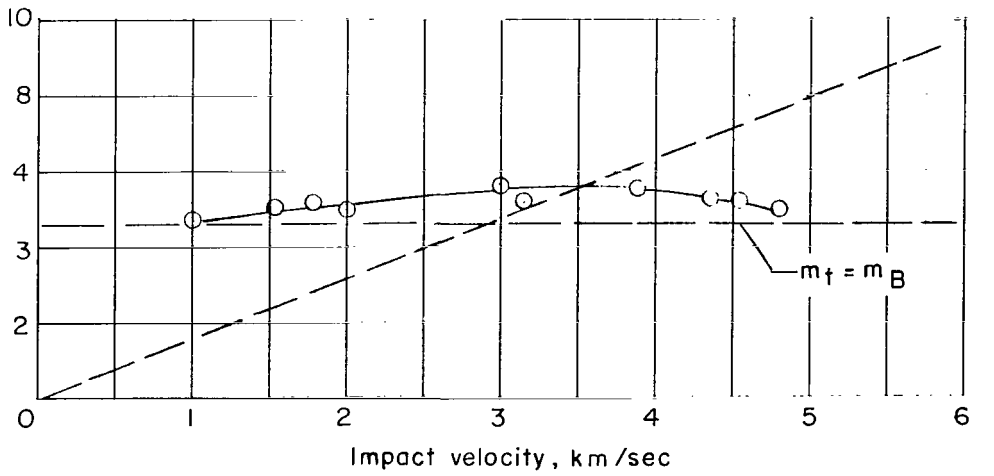

(c) t_B = 0.41 mm; m_B = 4.63 kg/m^2.

Figure 5.- Effect of bumper thickness on total penetration damage. Bumper material was lead; projectile was 1.59-mm-diameter aluminum sphere.

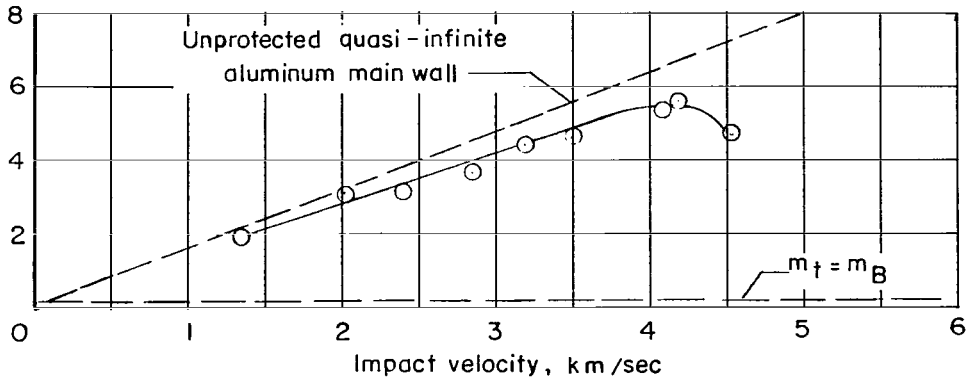

(a) t_B = 0.05 mm; m_B = 0.09 kg/m^2.

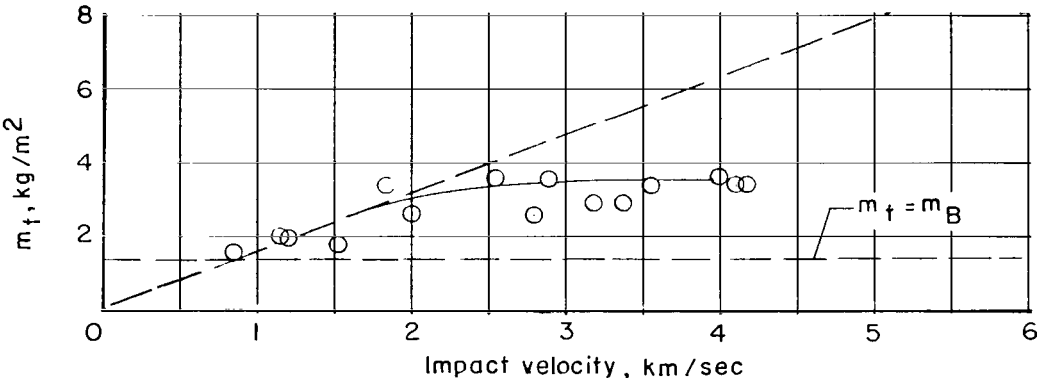

(b) t_B = 0.81 mm; m_B = 1.43 kg/m^2.

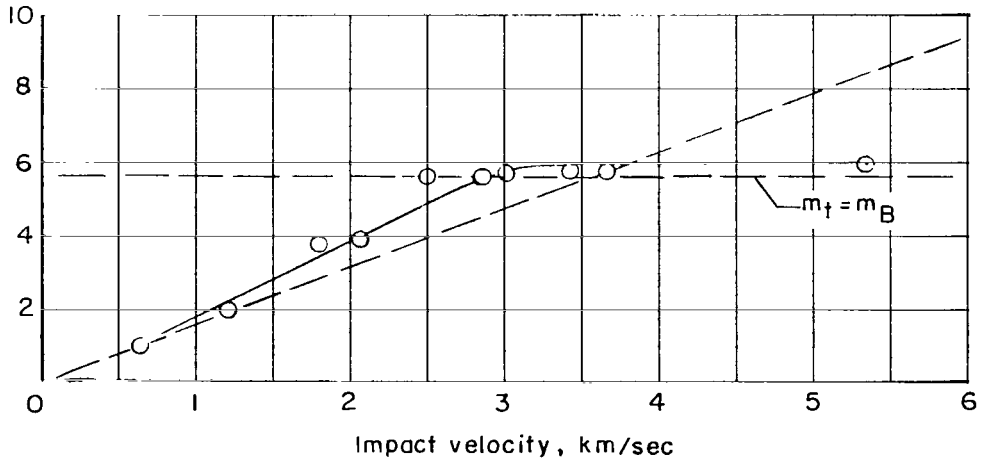

(c) t_B = 3.18 mm; m_B = 5.63 kg/m^2.

Figure 6.- Effect of bumper thickness on total penetration damage. Bumper material was magnesium AZ31B-0; projectile was 1.59-mm-diameter aluminum sphere.

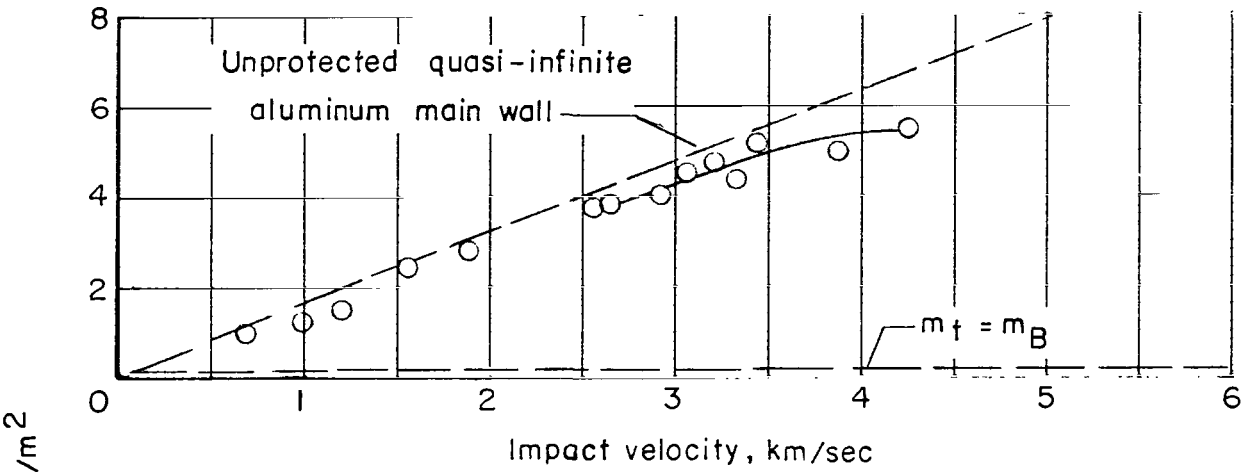

(a) t_B = 0.13 mm; m_B = 0.18 kg/m^2.

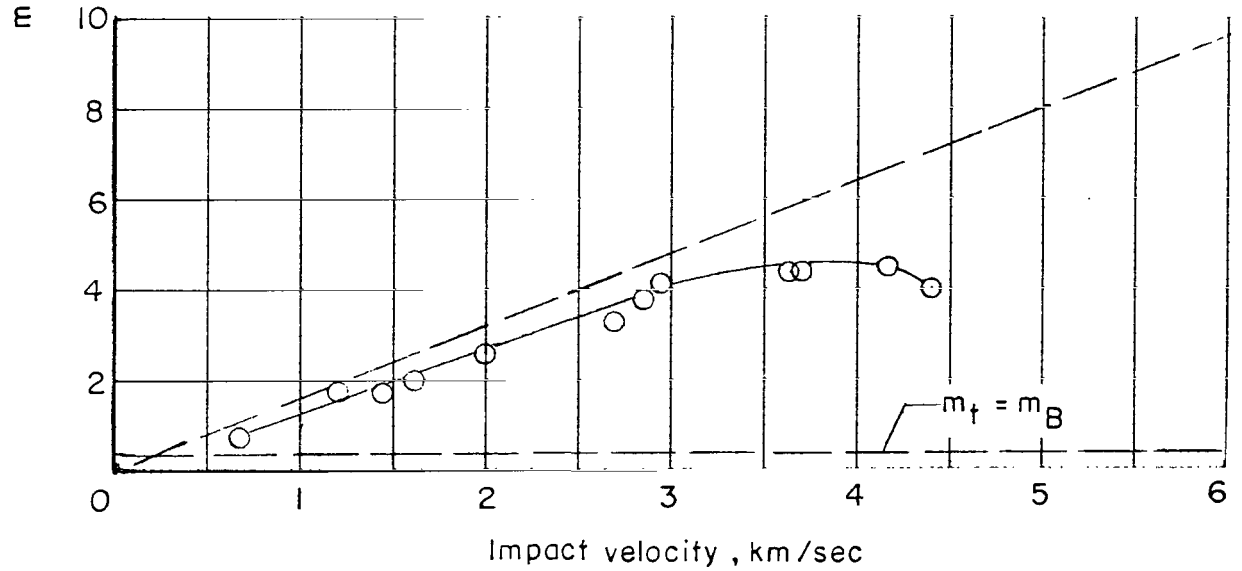

(b) t_B = 0.25 mm; m_B = 0.35 kg/m^2.

Figure 7.- Effect of bumper thickness on total penetration damage. Bumper material was Mylar; projectile was 1.59-mm-diameter aluminum sphere.

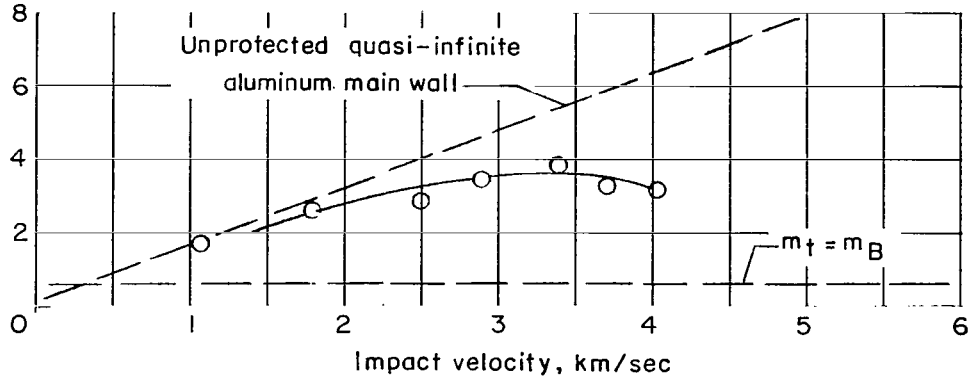

(a) t_B = 0.41 mm; m_B = 0.57 kg/m^2.

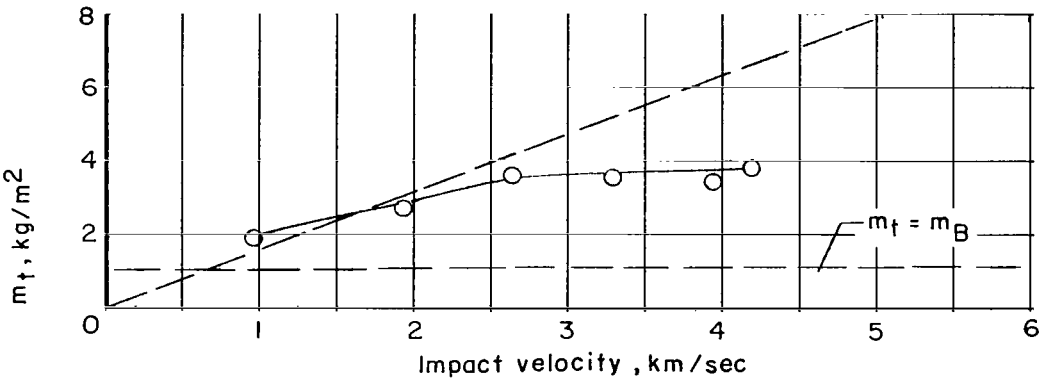

(b) t_B = 0.81 mm; m_B = 1.13 kg/m^2.

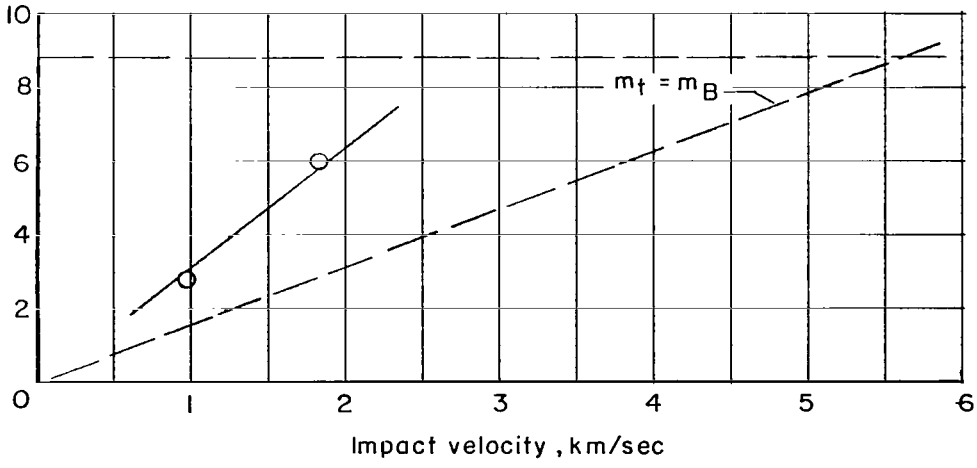

(c) t_B = 6.36 mm; m_B = 8.90 kg/m^2.

Figure 8.- Effect of bumper thickness on total penetration damage. Bumper material was neoprene, 40 durometer hardness; projectile was 1.59-mm-diameter aluminum sphere.

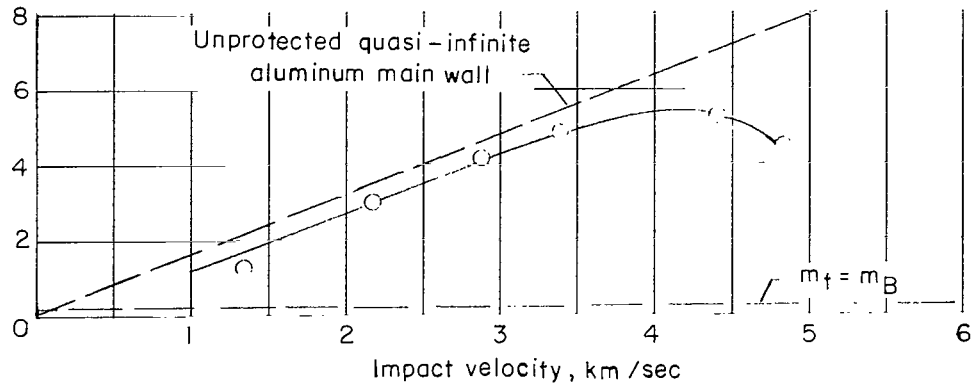

(a) t_B = 0.025 mm; m_B = 0.24 kg/m^2.

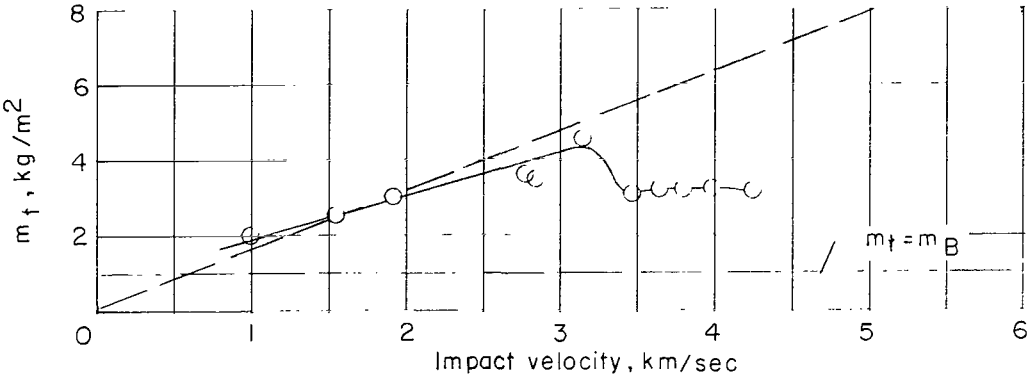

(b) t_B = 0.13 mm; m_B = 1.04 kg/m^2.

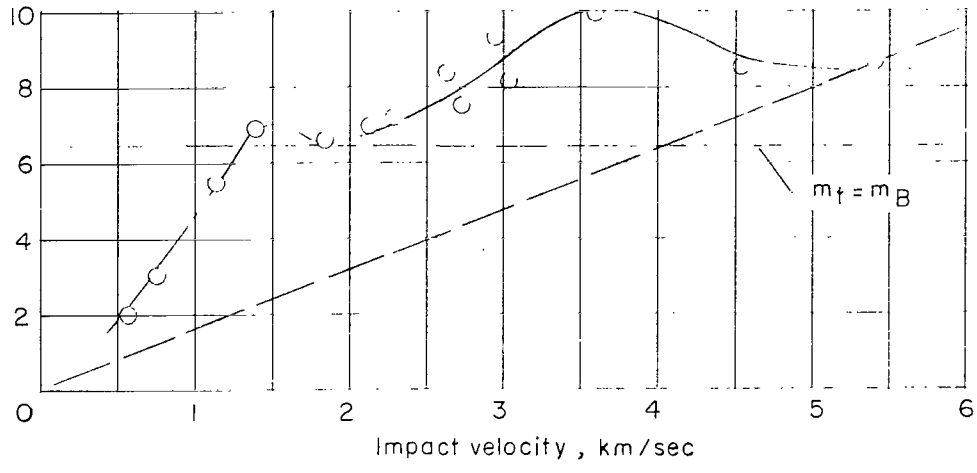

(c) t_B = 0.81 mm; m_B = 6.50 kg/m^2.

Figure 9.- Effect of bumper thickness on total penetration damage. Bumper material was stainless steel, 347 annealed; projectile was 1.59-mm-diameter aluminum sphere.

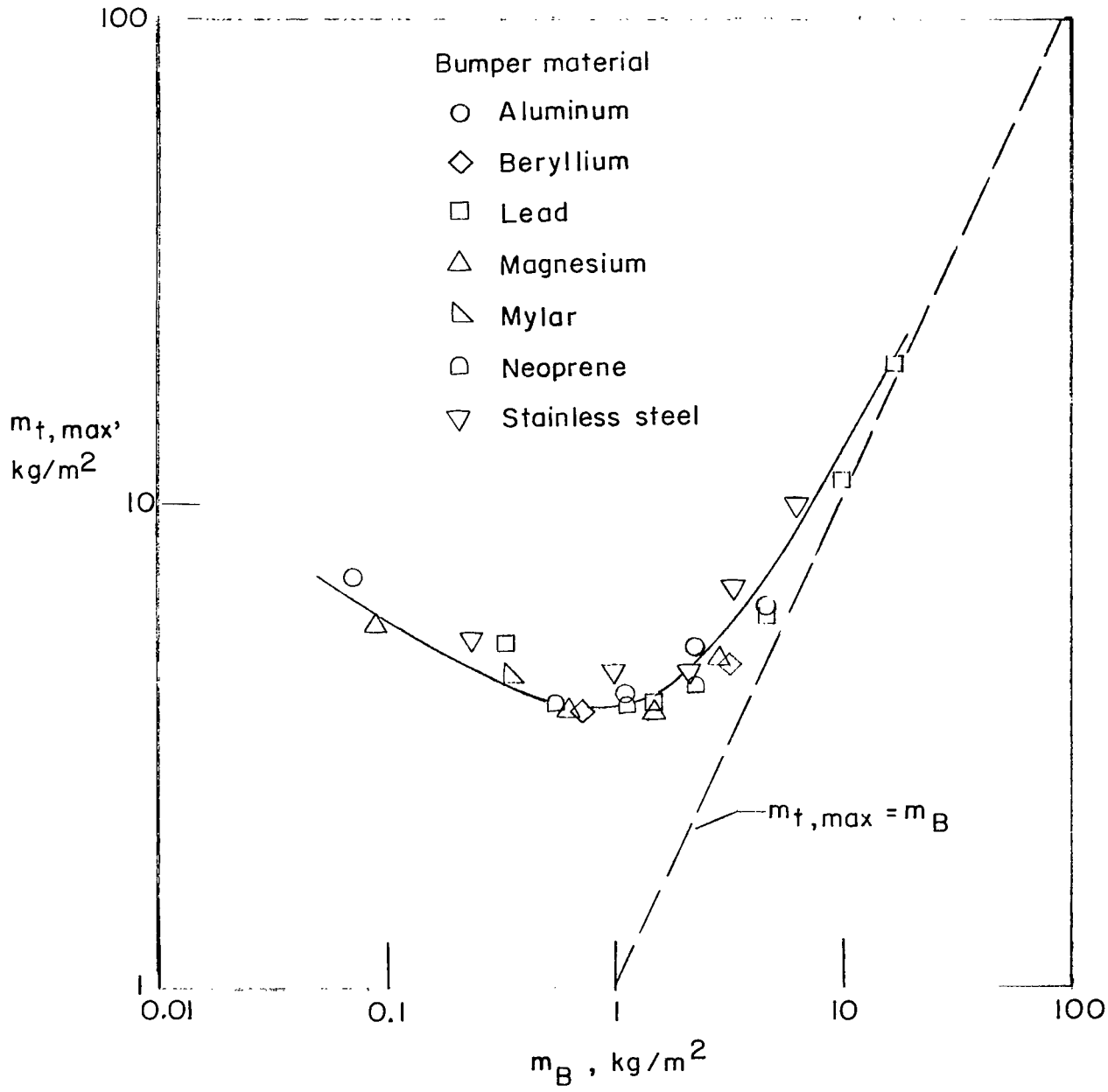

Figure 10.- Effect of bumper mass on the maximum total penetration damage. Projectile was 1.59-mm-diameter aluminum sphere. Quasi-infinite main wall was made of aluminum.

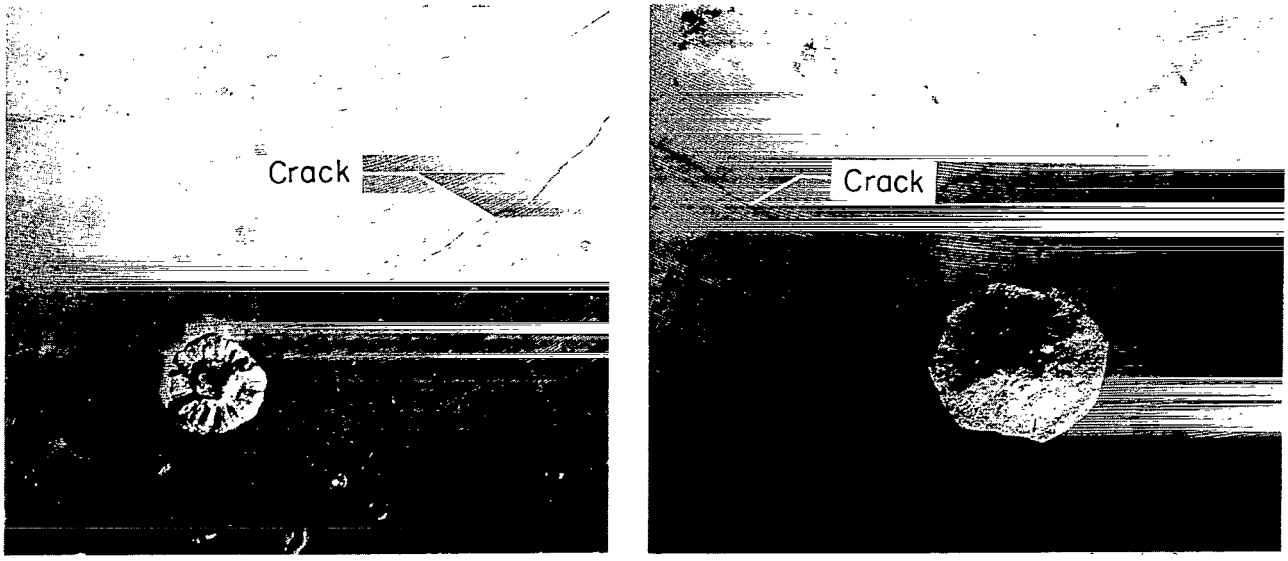

L-65-170

Figure 11.- Photographs showing crack and spallation cavity which developed in a partially penetrated beryllium bumper. The bumper thickness was 5.21 mm; the impact velocity was 3.57 km/s.

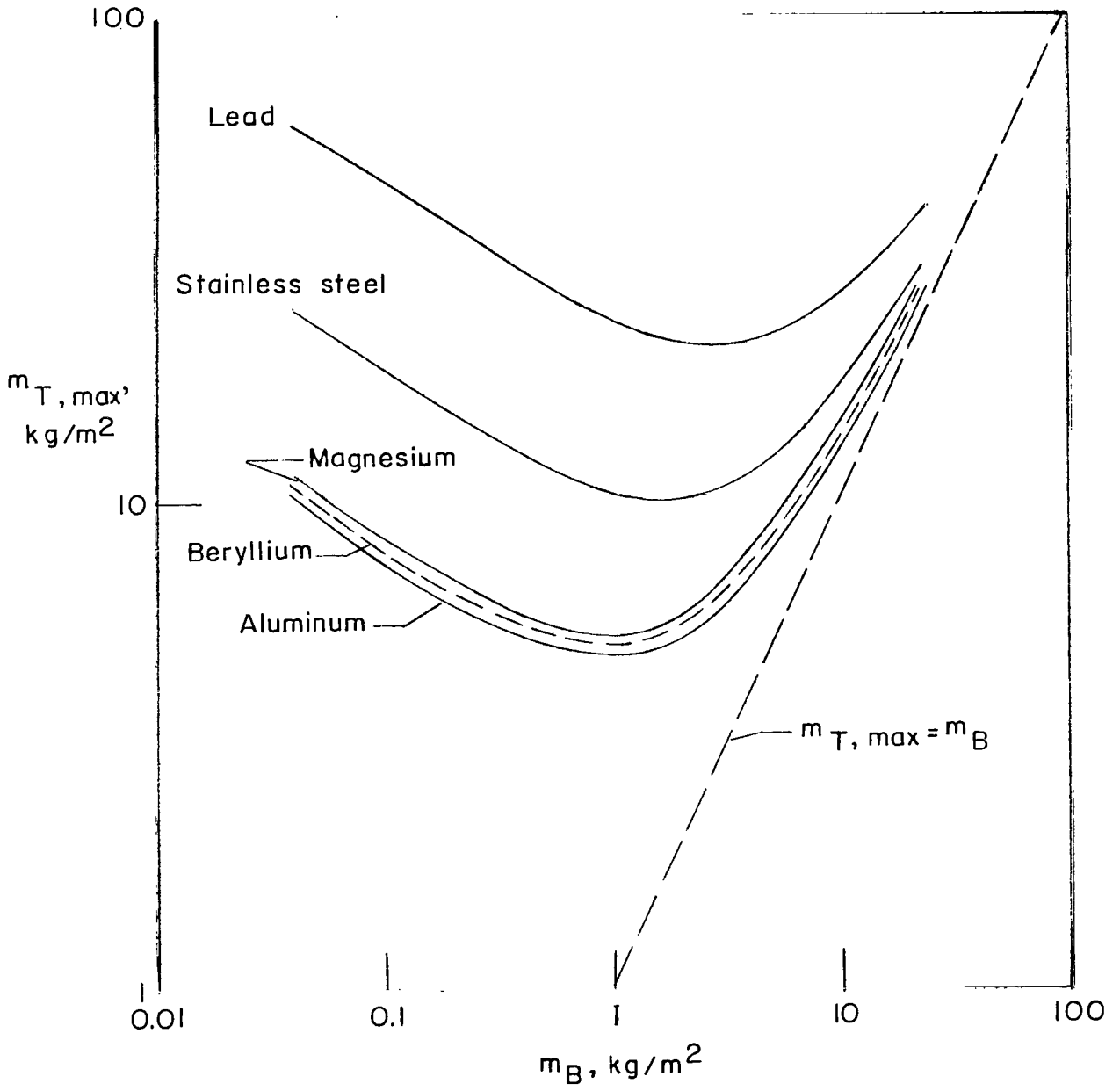

Figure 12.- Calculated effect of the main wall material on variation of the total mass required to defeat 1.59-mm-diameter aluminum projectiles with the bumper mass. Curves are independent of bumper material.

3/18/85
58

"The aeronautical and space activities of the United States shall be conducted so as to contribute . . . to the expansion of human knowledge of phenomena in the atmosphere and space. The Administration shall provide for the widest practicable and appropriate dissemination of information concerning its activities and the results thereof."

—NATIONAL AERONAUTICS AND SPACE ACT OF 1958

NASA SCIENTIFIC AND TECHNICAL PUBLICATIONS

TECHNICAL REPORTS: Scientific and technical information considered important, complete, and a lasting contribution to existing knowledge.

TECHNICAL NOTES: Information less broad in scope but nevertheless of importance as a contribution to existing knowledge.

TECHNICAL MEMORANDUMS: Information receiving limited distribution because of preliminary data, security classification, or other reasons.

CONTRACTOR REPORTS: Technical information generated in connection with a NASA contract or grant and released under NASA auspices.

TECHNICAL TRANSLATIONS: Information published in a foreign language considered to merit NASA distribution in English.

TECHNICAL REPRINTS: Information derived from NASA activities and initially published in the form of journal articles.

SPECIAL PUBLICATIONS: Information derived from or of value to NASA activities but not necessarily reporting the results of individual NASA-programmed scientific efforts. Publications include conference proceedings, monographs, data compilations, handbooks, sourcebooks, and special bibliographies.

Details on the availability of these publications may be obtained from:

SCIENTIFIC AND TECHNICAL INFORMATION DIVISION

NATIONAL AERONAUTICS AND SPACE ADMINISTRATION

Washington, D.C. 20546